Peracetic Acid Activated with Electro-Fe^{2+} Process for Dye Removal in Water

Deling Yuan [1,2], Kai Yang [1,2], Eryu Zhu [1,2], Xiongbo Li [1,2], Mengting Sun [1,2], Lichun Xiao [1,2,*], Qiga Hari [3,*] and Shoufeng Tang [1,2,4,*]

1   Hebei Key Laboratory of Heavy Metal Deep-Remediation in Water and Resource Reuse, School of Environmental and Chemical Engineering, Yanshan University, Qinhuangdao 066004, China; yuandl@ysu.edu.cn (D.Y.); yangkaiysu@163.com (K.Y.); zhueryu2022@163.com (E.Z.); lixbysu@163.com (X.L.); sunmt19@126.com (M.S.)
2   Hebei Key Laboratory of Applied Chemistry, School of Environmental and Chemical Engineering, Yanshan University, Qinhuangdao 066004, China
3   Heibei Province Low-Carbon and Clean Building Heating Technology Innovation Center, Hebei Key Laboratory of Green Construction and Intelligent Maintenance for Civil Engineering, School of Civil Engineering and Mechanics, Yanshan University, Qinhuangdao 066006, China
4   State Key Laboratory of Metastable Materials Science and Technology, School of Materials Science and Engineering, Yanshan University, Qinhuangdao 066004, China
*   Correspondence: xlc@ysu.edu.cn (L.X.); hariqiga@hotmail.com (Q.H.); tangshf@ysu.edu.cn (S.T.)

Abstract: An electro-Fe^{2+}-activated peracetic acid (EC/Fe^{2+}/PAA) process was established for organic dye removal in water. The operation factors such as the PAA dosage, Fe^{2+} amount, current density, and pH were investigated on methylene blue (MB) removal for the synergistic EC/Fe^{2+}/PAA system. Efficient MB decolorization (98.97% and 0.06992 min^{-1}) was achieved within 30 min under 5.4 mmol L^{-1} PAA, 30 μmol L^{-1} Fe^{2+}, 15 mA cm^{-2} current intensity, and pH 2.9. Masking tests affirmed that the dominating radicals were hydroxyl radicals (OH), organic radicals (CH$_3$CO$_2$·, CH$_3$CO$_3$·), and singlet oxygen (^{1}O$_2$), which were generated from the activated PAA by the synergetic effect of EC and Fe^{2+}. The influence of inorganic ions and natural organic matter on the MB removal was determined. Moreover, the efficacy of the EC/Fe^{2+}/PAA was confirmed by decontaminating other organic pollutants, such as antibiotic tetracycline and metronidazole. The studied synergy process offers a novel, advanced oxidation method for PAA activation and organic wastewater treatment.

Keywords: peracetic acid; ferrous ions; electrolysis; synergistic effect; dye elimination

1. Introduction

The effluents discharged from industries contain large amounts of organics, which can degrade the aquatic environment and bring adverse impacts for ecosystems [1,2]. Dye wastewater, as one of the representative organic wastewaters, contains many refractory compounds with high color and high concentration [3,4]. Because the traditional biological technologies are insufficient to treat the refractory organic contaminants in water, many physical and chemical methods have been developed over recent decades [5–7]. Advanced oxidation technologies (AOTs) can generate powerful reactive species—for example, the strong oxidative and nonselective hydroxyl radicals (·OH, E$_0$ = 1.9–2.7 V) [8], which can transform the macromolecular substances into small molecular substances and eventually mineralize them into CO$_2$ and H$_2$O [9]. Therefore, the application of AOTs in the treatment of organic dye wastewater has attracted widespread attention [10].

Peracetic acid (PAA) is a typical disinfector during water purification [11], which is a mixture of four ingredients, such as H$_2$O, PAA, H$_2$O$_2$, and acetic acid. As an electrophilic agent, PAA can attack electron-rich parts or functional groups in pollutants, so it can oxidize some organic substances, such as amino acids [12] and β-lactam antibiotics [13]. Owing to the mediocre redox potential of 1.76 V, PAA cannot directly degrade organic pollutants

that are resistant and persistent [14]. However, the peroxide bond of PAA is easily broken and activated due to the lower bond energy (38 kcal mol^{-1}) compared with that of H_2O_2 (51 kcal mol^{-1}) [15]. Therefore, researchers are becoming increasingly concerned about PAA activation methods [16]. The activated PAA could generate nonselective ·OH and selective organic free radicals (R-C·) including CH_3CO_2·, CH_3CO_3·, CH_3O_2·, and ·CH_3, etc., which could be effective for the elimination of organics in aqueous circumstances [17].

Previous research has shown that PAA can be activated by heat [18], ultraviolet [19], ultrasound [20,21], and cobalt metal ions and oxides (Co^{2+}, Co_3O_4, and $CoFe_2O_4$) [22–25]. Nevertheless, the above activation methods may have respective limitations—for example, high energy consumption and potential leaching toxicity [16]. Apart from these, Fe^{2+}-activating PAA is the most promising method, because iron species are eco-friendly and omnipresent in nature [26]. The inherent shortcomings of Fe^{2+}-activating PAA systems have hindered their development, such as the slow regeneration of Fe^{2+} and easy generation of iron precipitation, which is also the restrictive factor affecting the traditional Fenton process [27].

A number of studies have shown that EC can effectively promote Fe^{2+}/Fe^{3+} conversion through the cathode reaction for Fe^{2+} regeneration [28,29], forming the electro-Fenton process. The electro-Fenton process can generate H_2O_2 in situ and then enhance the production of ·OH radicals [30], thereby tremendously improving the degradation of pollutants. Moreover, many scientists have found that adding various peroxides (peroxydisulfate and peroxymonosulfate) into the electrolysis system could form a cooperative effect for removing organics in water [31–33]. Our previous study proved that electrolysis (EC) could effectively excite PAA for dye removal, but the activation efficiency still has room for improvement [34]. Hence, we propose the coupling of EC and Fe^{2+}-activating PAA (EC/Fe^{2+}/PAA) processes in this work.

The ternary synergistic system was expected to realize the efficient Fe^{2+}/Fe^{3+} cycle and PAA activation simultaneously. Methylene blue (MB), as a typical cationic dye, has complex and stable structures, which was selected to verify the performance of the synergistic system. The systematical study had the following aims: firstly, to research the enhancement of MB removal in the EC/Fe^{2+}/PAA process; secondly, to assess the effects of operation conditions and water constituents on the MB decolorization in the synergistic system; thirdly, to affirm the dominant reactive species for MB elimination; lastly, to propose a possible reaction mechanism of MB degradation in the EC/Fe^{2+}/PAA process.

2. Experimental

2.1. Materials and Reagents

Details of materials and reagents are introduced in Text S1 in the Supplementary Materials (SM).

2.2. Equipment and Procedure

A power source output a direct current to drive the EC system. The anode and cathode were platinum and graphite plates, separately, which were spaced 2 cm apart. The detailed information about the EC system is provided in Text S2 of Supplementary Materials. A beaker (100 mL) was applied as the reactor for the batch test. The designated concentrations of PAA and Fe^{2+} were introduced simultaneously to the reactor, which contained the target pollutant. The reaction was conducted at a temperature of 25 °C, with stable stirring. The initial pH was regulated through the addition of NaOH and H_2SO_4. The EC reaction started after switching on the power. Sampling was performed at a fixed time node, and 1 mL $Na_2S_2O_3$ solution was added for quenching active species before the concentration was determined. Different reactive species scavengers were added to the reactor separately to investigate the reaction mechanism in the masking tests.

2.3. Analytical Methods

The concentrations of MB, methyl orange (MO), and rhodamine B (RhB) were determined by the spectrophotometric method at 664, 465, and 554, nm, respectively. The metronidazole (MTZ) and tetracycline (TCH) concentrations were measured by High-Performance Liquid Chromatography (HPLC). The degradation byproducts of MB were investigated by HPLC combined with mass spectrum (MS). The amounts of iron ions were determined by the phenanthroline spectrophotometric method [35]. The change in PAA was measured by the N,N-diethyl-p-phenylenediamine (DPD) colorimetric method [36]. The H_2O_2 concentration was quantified through titanium potassium oxalate colorimetry [35].

2.4. Energy Efficiency

The calculated electrical energy per order (EE/O) was denoted as electrical energy consumption by the following equation [37]:

$$\frac{EE}{O} = \frac{U \times I \times T}{V \times 60 \times \log(C_0 / C)} \tag{1}$$

where EE/O represents the electrical energy (kWh) consumed for removing the pollutant by an order of magnitude in a significant volume (V, L) of wastewater and a certain time (T, min); U and I stand for the voltage (V) and current (A), respectively; C_0 and C indicate the beginning and ending contaminant concentrations, respectively.
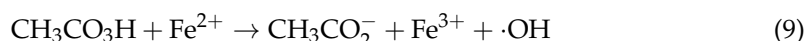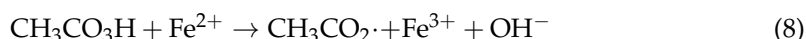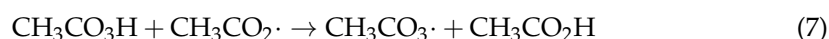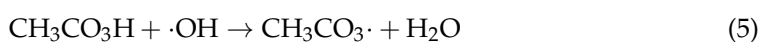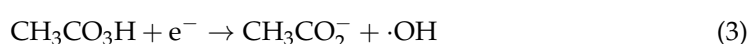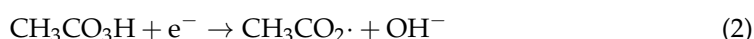
3. Results and Discussion

3.1. Performance of EC/Fe^{2+}/PAA Process

The decolorizations of MB in the PAA, Fe^{2+}, Fe^{2+}/PAA, EC/Fe^{2+}, EC, EC/PAA, and EC/Fe^{2+}/PAA systems are comprehensively compared in Figure 1a. After 60 min of reaction, the decolorization ratios of MB in the PAA alone and sole Fe^{2+} systems were only 5.13% and 7.26%, respectively. In the Fe^{2+}/PAA system, the decolorization of MB reached 35.15%. The removals of MB in the EC, EC/Fe^{2+}, and EC/PAA systems were 54.55%, 52.24%, and 66.64%, respectively. However, the decoloring performance was greatly improved for the EC/Fe^{2+}/PAA process, and the elimination efficiency of MB increased to 98.97%, showing a significant synergistic effect. In Figure 1b, the kinetic fitting results indicate that the reaction rate constant of EC/Fe^{2+}/PAA reached 0.06992 min^{-1}, which was obviously higher than other processes (the PAA and Fe^{2+} were both fitted by a zero-order kinetic model, and other systems were all fitted through a pseudo-first-order kinetic model). The above results demonstrate that the ternary synergistic process could remarkably promote the decolorization efficiency and rate of MB.
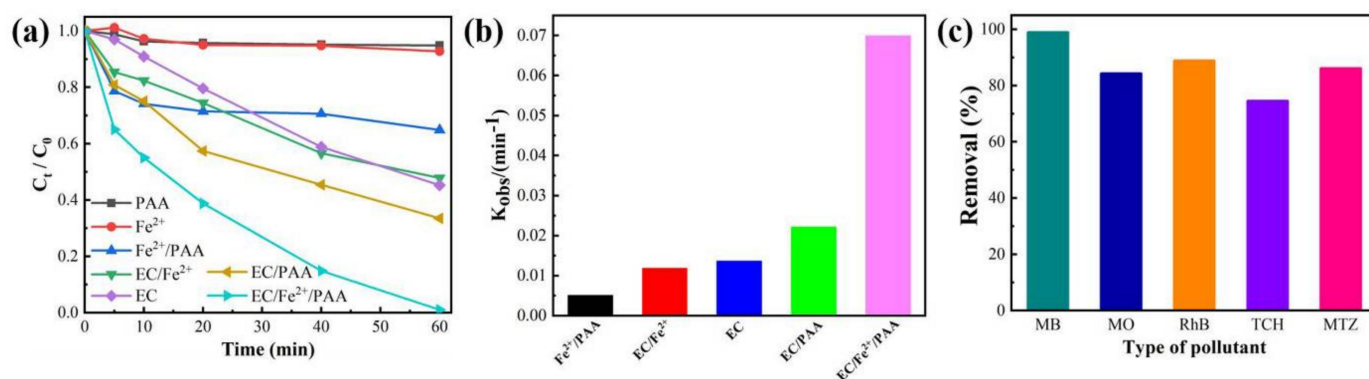
Figure 1. Decolorization ratio (**a**) and reaction rate constant (**b**) of MB in various systems. (**c**) Diverse organic pollutant removal in EC/Fe^{2+}/PAA system. Experimental conditions: $[MB]_0 = [MO]_0 = [RhB]_0 = [TCH]_0 = [MTZ]_0 = 20$ mg L^{-1}, $[Fe^{2+}]_0 = 30$ μmol L^{-1}, $[PAA]_0 = 5.4$ mmol L^{-1}, $[H_2O_2]_0 = 11.25$ mmol L^{-1}, $[NaNO_3] = 30$ mmol L^{-1}, pH = 2.9, $j = 15$ mA cm^{-2}.

In the EC/PAA system, the electron-donating condition for the cathode could activate PAA (Equations (2) and (3)) [38]. Furthermore, the ·OH produced by the electron loss reaction on the anode not only could remove the MB (Equation (4)) [39], but also activate PAA to generate $CH_3CO_3.$ and $CH_3CO_2.$ for the oxidation of organic pollutants (Equations (5)–(7)) [20]. Meanwhile, the electron transfer on the surface of the electrode could directly oxidize MB. However, the main drawback of this system is that the reactions of PAA activation and radical generation are confined to the electrode surface. In the Fe^{2+}/PAA process, the transition metal ions of Fe^{2+} were often used as an activator, which could activate PAA to generate organic free radicals and ·OH (Equations (8) and (9)) [24]. However, the generated Fe^{3+} was difficult to reduce and easily produced iron sludge, leading to insufficient oxidation for MB removal.

$$CH_3CO_3H + e^- \rightarrow CH_3CO_2\cdot + OH^- \tag{2}$$

$$CH_3CO_3H + e^- \rightarrow CH_3CO_2^- + \cdot OH \tag{3}$$

$$H_2O \rightarrow \cdot OH + H^+ + e^- \tag{4}$$

$$CH_3CO_3H + \cdot OH \rightarrow CH_3CO_3\cdot + H_2O \tag{5}$$

$$CH_3CO_3\cdot + CH_3CO_3\cdot \rightarrow 2CH_3CO_2\cdot + O_2 \tag{6}$$

$$CH_3CO_3H + CH_3CO_2\cdot \rightarrow CH_3CO_3\cdot + CH_3CO_2H \tag{7}$$

$$CH_3CO_3H + Fe^{2+} \rightarrow CH_3CO_2\cdot + Fe^{3+} + OH^- \tag{8}$$

$$CH_3CO_3H + Fe^{2+} \rightarrow CH_3CO_2^- + Fe^{3+} + \cdot OH \tag{9}$$

Nevertheless, after adding the Fe^{2+} to the EC/PAA system, the combined effect of the electro-Fenton and PAA activation reactions could promote the oxidative radicals' generation and then enhance the dye elimination. Furthermore, the synergistic effect could extend the oxidation and activation reactions from the electrode surfaces to the entire solution, greatly improving the capability of this system. In addition, the generated Fe^{3+} could be reduced to Fe^{2+} by obtaining electrons at the cathode (Equation (10)) [32], realizing the reuse of Fe^{2+} for sustainable PAA activation.

$$Fe^{3+} + e^- \rightarrow Fe^{2+} \tag{10}$$

To prove that the EC/Fe^{2+}/PAA system is effective in removing diverse organic pollutants, three reactive dyes (MB, MO, and RhB) and two antibiotics (TCH and MTZ) were selected for the elimination tests [40]. As illustrated in Figure 1c, the significant abatement of MB, MO, RhB, TCH, and MTZ by the EC/Fe^{2+}/PAA process was observed, and their removal efficiencies reached 98.89%, 84.33%, 88.88%, 74.53%, and 86.15% during 60 min, respectively, certifying the effectiveness of the synergy process for the common organic contaminants' decontamination. These organic compounds contain methyl and hydroxyl groups, and these electro-rich functional groups could be susceptible to reaction with R-C· via electron transferring [41].

3.2. Influencing Factors for EC/Fe^{2+}/PAA Process
3.2.1. PAA Dosage

The effect of different PAA dosages for MB decolorization during the EC/Fe^{2+}/PAA process was researched (Figure 2a). The MB removal was enhanced from 61.26% to 91.80% at 60 min with the PAA dosage augmented from 0.9 to 5.4 mmol L^{-1}. Boosting the PAA dose could supply the substrate of active species generation for removing MB. Nevertheless, while the PAA amount was raised to 9.0 mmol L^{-1}, the MB elimination was inhibited slightly, demonstrating that the superfluous PAA could not continuously improve the MB oxidation. This is because the H_2O_2 in PAA has a negative impact on the ·OH radical

through scavenging effects [18], which could impact the PAA activation and then inhibit the dye elimination. Therefore, the optimal concentration of PAA was set at 5.4 mmol L^{-1}.
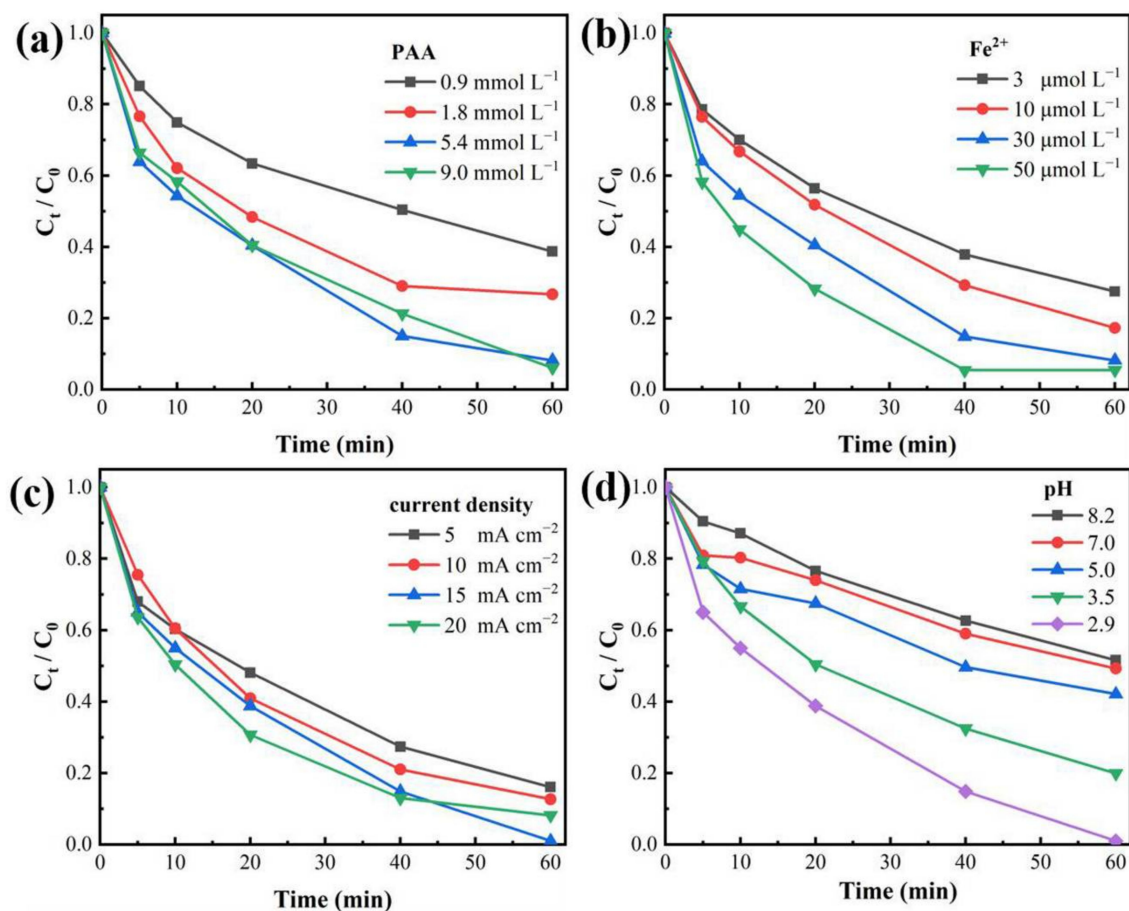
Figure 2. Decolorization ratio of MB under different reaction conditions: (**a**) PAA dosage, (**b**) Fe^{2+} dosage, (**c**) current density, and (**d**) solution pH. Experimental conditions: $[MB]_0 = 20$ mg L^{-1}, $[Fe^{2+}]_0 = 30$ μmol L^{-1}, $[PAA]_0 = 5.4$ mmol L^{-1}, $[H_2O_2]_0 = 11.25$ mmol L^{-1}, $[NaNO_3] = 30$ mmol L^{-1}, pH = 2.9, $j = 15$ mA cm^{-2}.

3.2.2. Fe^{2+} Dosage

The effect of Fe^{2+} dosage on MB decolorization was evaluated (Figure 2b). With the Fe^{2+} concentration increasing from 3 to 30 μmol L^{-1}, the decolorization efficiency of MB was enhanced from 72.48% to 91.80% within 60 min, which indicated that an appropriate increase in Fe^{2+} dosage could catalyze PAA more efficiently and rapidly, hence strengthening the reactive radicals' formation and the MB removal. When the Fe^{2+} dosage was raised to 50 μmol L^{-1}, the MB removal ratio was not enhanced at 60 min, but the decolorization rate was improved obviously. Considering the cost saving, the suitable concentration of Fe^{2+} was chosen as 30 μmol·L^{-1}.

3.2.3. Current Intensity

As can be seen from Figure 2c, with the current intensity rising from 5 to 15 mA cm^{-2}, the decolorization ratio of MB was augmented from 84.74% to 93.73%. The stronger current is a benefit for the ·OH formation on the anode surface and Fe^{3+} reduction on the cathode surface [42,43], which could promote PAA activation and the oxidation of organics. Nevertheless, as the current was enhanced to 20 mA cm^{-2}, the decolorization of MB incurred a slight drop. This phenomenon reflects the fact that the exorbitant current density would improve the electrolysis of water, and the generated O_2 at the anode would accelerate

the oxidation of Fe^{2+} to Fe^{3+} (Equation (11)) [44], then suppressing the PAA activation and dye removal. Hence, the suitable current density value was set to be 15 mA cm^{-2}.

$$2H_2O \rightarrow 4H^+ + O_2 + 4e^- \tag{11}$$

3.2.4. Initial pH

The pH condition could impact the form and redox potential of PAA. Thus, the effects of different solution pH on the MB removal were explored (Figure 2d). The result showed that acidic conditions were more conducive to the decolorization of MB. Under the alkaline condition (pH = 8.2), the removal of MB was only 56.03%. Nevertheless, the decolorization reached 98.97% at pH 2.9. The pKa value of PAA is approximately 8.2 [15]. The lower the pH, the more protonated PAA (PAA^0) was the dominant form in solution [16]. When the pH was near to 8.2, the PAA was prone to self-decomposition and hydrolysis, and the proportion of deprotonated PAA (PAA^-) would be enhanced in solution [16]. The oxidizing ability of PAA^0 is higher than that of PAA^- [12]. Moreover, compared to PAA^-, the PAA^0 more easily accepts electrons, and is more liable to be activated by Fe^{2+} [45]. In addition, the Fe^{3+}/Fe^{2+} cycle becomes more difficult as the pH increases [46]. Therefore, the acidic environment was conducive to the removal of MB in the $EC/Fe^{2+}/PAA$ process.

3.3. Mechanism of EC/Fe^{2+}/PAA Process

3.3.1. Scavenging Test

Radical quenching experiments were employed to distinguish the various active substances in the $EC/Fe^{2+}/PAA$ process. Five scavengers were employed, namely tert-butyl alcohol (TBA), methanol (MeOH), phenol, P-benzoquinone (p-BQ), and L-Histidine (L-His). TBA is a common scavenging agent for ·OH on account of the fast reaction rate (5×10^8 M^{-1} s^{-1}) with ·OH [36]. MeOH is a hydrophilic agent, which can quench ·OH, CH_3CO_2, and CH_3CO_3 at the same time [41]. Phenol is a hydrophobic chemical, which can react quickly with OH, CH_3CO_2·, and CH_3CO_3· near the electrode [39]. p-BQ is an excellent masking agent for superoxide anions ($O_2^{·-}$) [47]. L-Histidine is a typical inhibiting agent for singlet oxygen ($^1O_2$) [47].

A summary of the scavenging results is given in Figure 3a. Overall, 98.97% of MB was removed in the absence of a scavenger. The MB decay declined by approximately 6.04% with the addition of p-BQ, proving the inappreciable role of $O_2^{·-}$ in this system. The suppression of MB decolorization was more prominent with the existence of L-His and the removal ratio of MB dropped to 80%, which proved that the $^1O_2$ plays a non-negligible role in MB elimination (Equations (12) and (13)) [48,49]. Adding excess MeOH and TBA cannot entirely restrain the MB decolorization, and the decolorization was reduced to 72.70% and 60.15%, respectively. However, when 50 mol L^{-1} of phenol was added, the inhibition effect on the MB removal became acute, and the decolorization was reduced to 28.49%. This result indicated that the free radicals on the electrode surface could play an important role in MB elimination. Hence, the major active species for MB removal were ·OH, CH_3CO_2·, CH_3CO_3·, and $^1O_2$ in the $EC/Fe^{2+}/PAA$ system. Moreover, the presence of phenol had a more obvious suppression influence than TBA and MeOH, demonstrating that the PAA activation and related radicals' reactions for MB elimination mostly originated from the electrode surface. In addition, the above results confirmed that the PAA was primarily activated by the EC system, as observed in Figure 1a.

$$O_2^{·-} + ·OH \rightarrow HO^- + {}^1O_2 \tag{12}$$

$$O_2^{·-} + 2H^+ \rightarrow H_2O_2 + {}^1O_2 \tag{13}$$
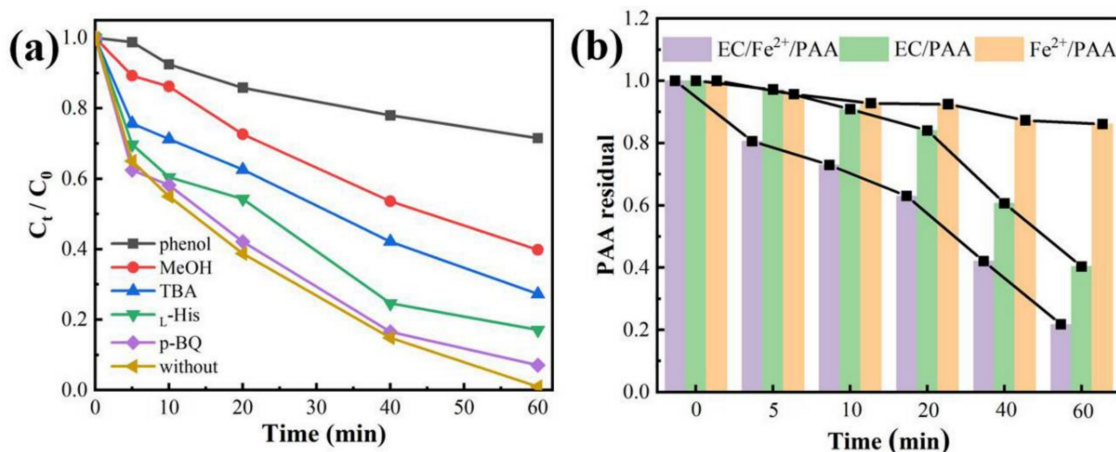
Figure 3. MB removal under various radical quenching agents in EC/Fe^{2+}/PAA (**a**). Remaining amount of PAA under different systems (**b**). Experimental conditions: [MB]$_0$ = 20 mg L^{-1}, [Fe^{2+}]$_0$ = 30 µmol L^{-1}, [PAA]$_0$ = 5.4 mmol L^{-1}, [H$_2$O$_2$]$_0$ = 11.25 mmol L^{-1}, TBA = 6 mol L^{-1}, MeOH = 10 mol L^{-1}, phenol = 50 mmol L^{-1}, p-BQ = 200 µmol L^{-1}, $_L$-His = 200 µmol L^{-1}, [NaNO$_3$] = 30 mmol L^{-1}, pH = 2.9, j = 15 mA cm^{-2}.

3.3.2. PAA Utilization Rate

As the major precursor of active radicals in the EC/Fe^{2+}/PAA is PAA, monitoring the residual PAA concentration can reflect its activation efficiency. As presented in Figure 3b, the remaining proportion of PAA (the remaining PAA to initial PAA) in the three systems (Fe^{2+}/PAA, EC/PAA, and EC/Fe^{2+}/PAA) decreased with the increase in time and the downward trend was enhanced significantly. After 60 min of reaction, only 13.87% of PAA was consumed in the Fe^{2+}/PAA process, and 59.62% of PAA was decomposed in the EC/PAA system, revealing that the PAA's activation ability for the EC process was stronger than that for the Fe^{2+} system. The highest decomposition ratio of PAA was significantly increased to 78.23% for the EC/Fe^{2+}/PAA process, which was higher than that for the other two systems. This result clearly shows that the EC/Fe^{2+}/PAA system yields an excellent synergistic effect for PAA activation. In summary, the above phenomena were in agreement with the outcomes of MB removal and radical quenching tests.

3.3.3. Trend of Fe Irons

Fe^{2+} is a crucial element in EC/Fe^{2+}/PAA, which could not excite PAA, but also plays the role of catalyst in the electro-Fenton process. The changes in the Fe^{2+} and Fe^{3+} concentration were compared in the Fe^{2+}/PAA and EC/Fe^{2+}/PAA systems (Figure 4). As displayed in Figure 4a, the Fe^{2+} content decreased rapidly with the increase in Fe^{3+} within 5 min in the Fe^{2+}/PAA process, and the trend tended towards becoming stable after 10 min. At the same time, the total Fe amount only fell by 2% during the 60 min reaction. The results were mainly ascribed to the fast depletion of Fe^{2+}, the activation of PAA, and the ineffective conversion of Fe^{3+} to Fe^{2+}, once again verifying the outcome of MB removal shown in Figure 1a. However, as illustrated in Figure 4b, in the EC/Fe^{2+}/PAA process, the concentration of Fe^{2+} remained at a higher level than that in Fe^{2+}/PAA, and the amount of Fe^{3+} also maintained a lower level than that of Fe^{2+}/PAA. These results prove that Fe^{3+} could be continuously converted into Fe^{2+} under the effect of cathode electron transfer, resulting in a higher concentration of Fe^{2+} in the system. Moreover, the total Fe content in the EC/Fe^{2+}/PAA process was decreased to 80%, which was more remarkable compared with the Fe^{2+}/PAA. In the electrolysis system, the Fe ions could undergo a reduction reaction by receiving electrons from the cathode, and then be deposited on the surface of the cathode, resulting in a decline in the total Fe concentration [39].
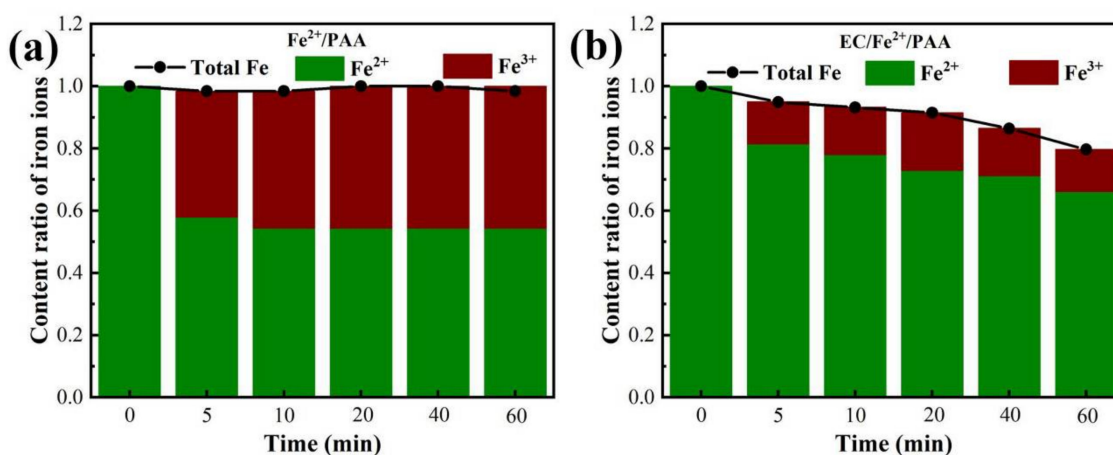
Figure 4. Changes in Fe content in Fe^{2+}/PAA process (**a**) and EC/Fe^{2+}/PAA (**b**). Experimental conditions: $[MB]_0 = 20$ mg L^{-1}, $[Fe^{2+}]_0 = 30$ μmol L^{-1}, $[PAA]_0 = 5.4$ mmol L^{-1}, $[H_2O_2]_0 = 11.25$ mmol L^{-1}, $[NaNO_3] = 30$ mmol L^{-1}, pH = 2.9, $j = 15$ mA cm^{-2}.

3.4. MB Degradation Mechanism

The UV–visible spectrum was used to confirm the decolorization of MB in the EC/Fe^{2+}/PAA. As can be seen from Figure S1 of Supplementary Materials, the absorption peak at 664 nm gradually disappeared within 60 min [50], indicating that the chromogenic group of sulfhydryl (-S-) of MB was destroyed by the free radicals of EC/Fe^{2+}/PAA [51].

The TOC removal for MB was determined during the collaborative process. As seen in Figure S2 in Supplementary Materials, the TOC almost remained unchanged in the 120 min treatment. This result indicated that the application of activated PAA could increase the TOC, which is derived from the residual PAA and acetic acid [34]. Hence, the PAA-related process combined with the biological treatment could be a promising option because the increased TOC is a good carbon source for microorganisms [22,52].

The HPLC-MS spectra of MB before and after synergistic oxidation are presented in Figure S3 of Supplementary Materials. The peak of $m/z = 284$ was attributed to the MB, which was evidently decreased after 60 min reaction, corroborating the decomposition of MB. Based on the results of MS analyses, the possible degradation pathway of MB was suggested (Figure 5). Initially, the cation of MB (MB^+) could be formed via the electron transfer between MB and $CH_3CO_2\cdot$ or $CH_3CO_3\cdot$. Next, the MB^+ would rapidly react with H_2O or O_2 to produce hydroxylated byproduct No. 1 through the reactions of hydroxyl extraction or addition [53]. The MB could be demethylated to generate byproduct No. 2 under the action of ·OH. In addition, the central aromatic ring of MB could also be opened by ·OH to produce byproduct No. 3, which contained amino (-NH_2) and sulfoxide (C-S (=O)-C) functional groups [54]. The methylated byproduct No. 2 could also be further demethylated to form byproduct No. 4 after losing four methyl groups. After this, the N = C bond and sulfhydryl group of byproduct No. 4 could be broken down to form byproducts No. 5 and No. 6. The byproduct No. 4 could generate the hydroxylated byproduct No. 7 via the attack of ·OH. The benzene ring of byproduct No. 6 was cleaved to produce small-molecule byproduct No. 8, which was further split into small-molecule fragment byproduct No. 9. The hydroxylated byproduct No. 1 also could be broken to form byproducts No. 5 and No. 10 through the ring opening reaction under the function of ·OH. The byproduct No. 3 could be hydroxylated to form byproduct No. 11, and then demethylated to produce byproduct No. 12, and the sulfoxide was cracked to generate byproduct No. 13 [49,55]. Finally, these degradation intermediates could be further oxidized and converted to CO_2, H_2O, SO_4^{2-}, and NO_3^- [56].
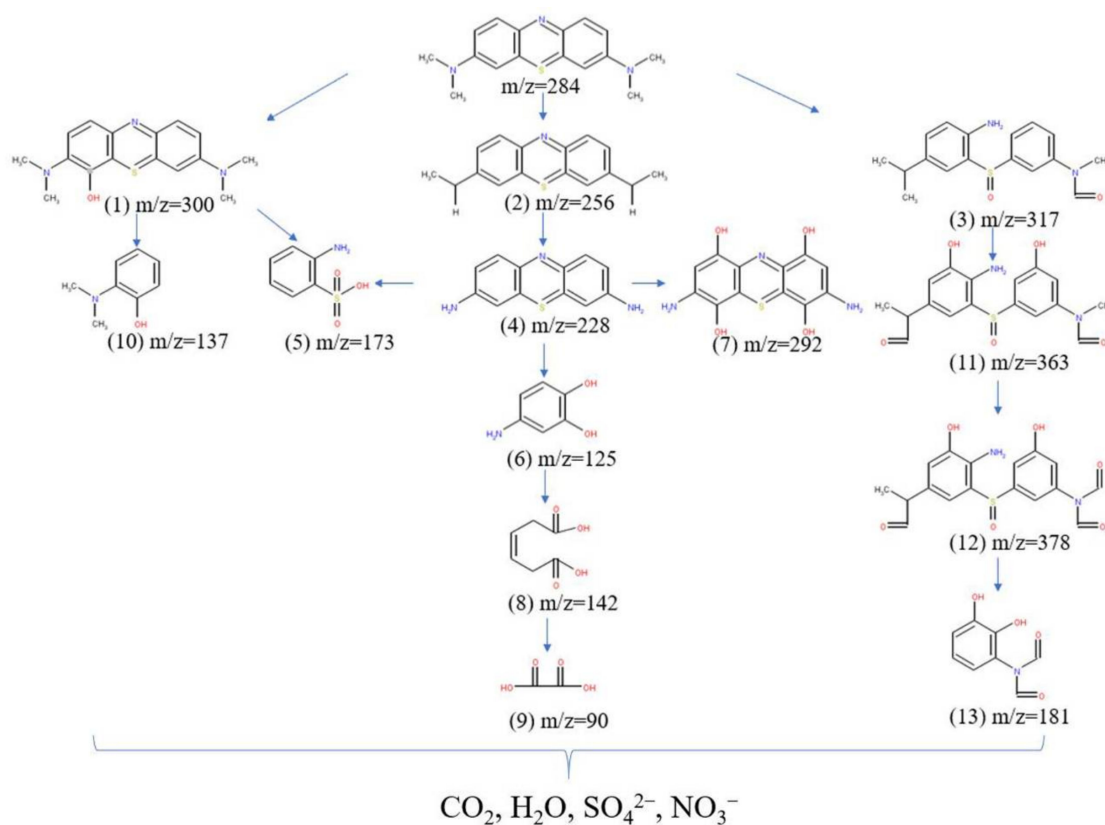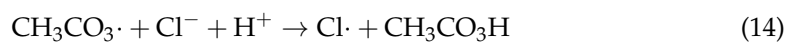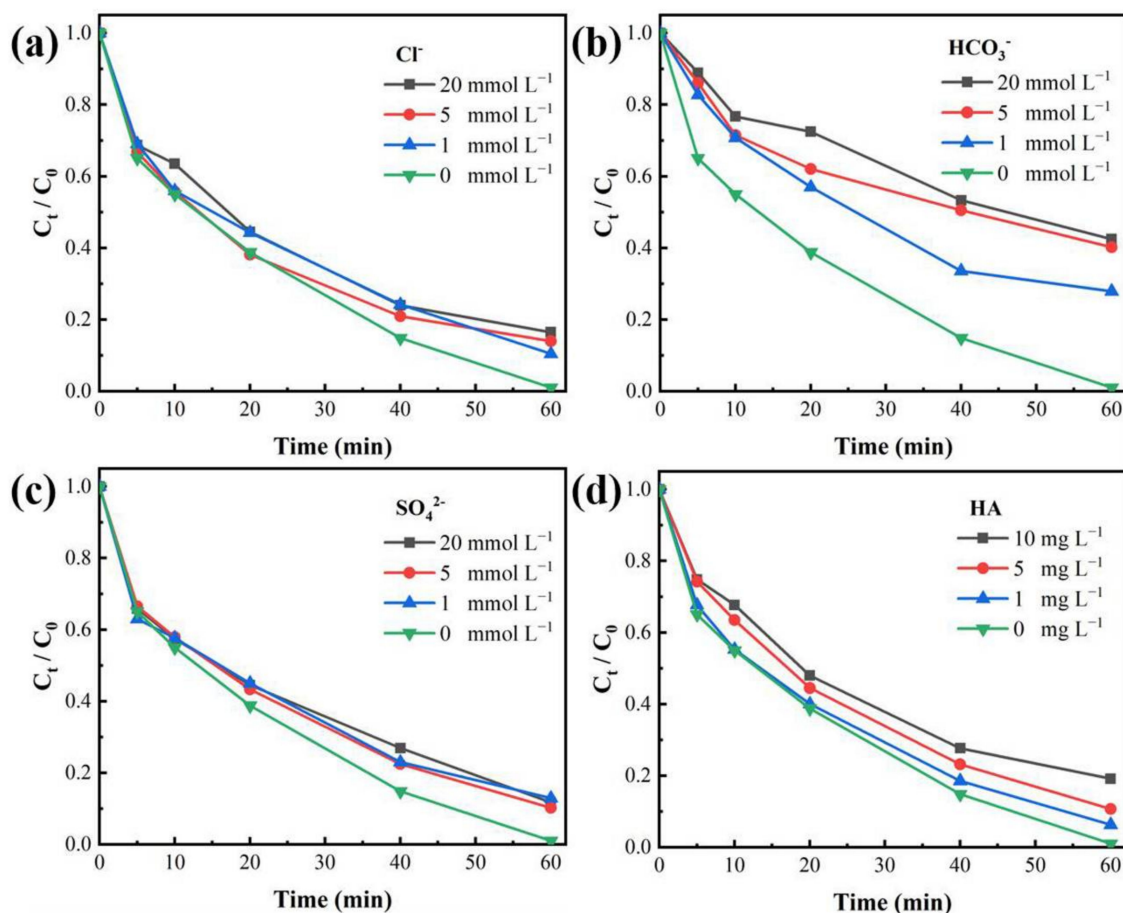
Figure 5. Possible degradation pathway in EC/Fe^{2+}/PAA.

3.5. Water Matrices Effects

The effect of Cl$^-$ on the MB removal in the EC/Fe^{2+}/PAA was explored. As seen in Figure 6a, the existence of Cl$^-$ (1–20 mmol L^{-1}) had a certain passive effect on the MB elimination, and the removal efficiency decreased from 98.97% to 83.47%. Chloride ions can scavenge free radicals, resulting in the generation of reactive chlorine species (Cl·, Cl$_2$·$^-$, and HClO·$^-$, Equations (14)–(18)) [36,57], whose oxidation capacities were lower than those of reactive species generated in the PAA activation. In addition, the coexisting iron and chloride ions could oxidize Fe^{2+} to Fe^{3+} and form Fe(Cl)$^{2+}$ and FeCl$_2$$^+$ complexes (Equation (19)) [14], harming the reaction of Fe^{2+} activating PAA.

$$CH_3CO_3\cdot + Cl^- + H^+ \rightarrow Cl\cdot + CH_3CO_3H \tag{14}$$

$$Cl^- + \cdot OH \rightarrow HClO\cdot^- \tag{15}$$

$$HClO\cdot^- + H^+ \rightarrow Cl\cdot + H_2O \tag{16}$$

$$Cl^- + Cl\cdot \rightarrow Cl_2^- \tag{17}$$

$$Cl\cdot + Cl\cdot \rightarrow Cl_2 \tag{18}$$

$$Fe^{2+} + Cl\cdot \rightarrow Fe^{3+} + Cl^- \tag{19}$$

Figure 6. Effects of presence of (**a**) Cl^-, (**b**) HCO_3^-, (**c**) SO_4^{2-}, and (**d**) HA (0–10 mg L^{-1}) on MB decolorization in $EC/Fe^{2+}/PAA$ process. Experimental conditions: $[MB]_0 = 20$ mg L^{-1}, $[Fe^{2+}]_0 = 30$ µmol L^{-1}, $[PAA]_0 = 5.4$ mmol L^{-1}, $[H_2O_2]_0 = 11.25$ mmol L^{-1}, $[NaNO_3] = 30$ mmol L^{-1}, pH = 2.9, $j = 15$ mA cm^{-2}.

The effect of bicarbonate ions on MB removal in the $EC/Fe^{2+}/PAA$ was investigated (Figure 6b). Increasing bicarbonate ions amount led to the strong inhibition of the MB removal, and when the HCO_3^- was increased to 20 mmol L^{-1}, the decolorization ratio was reduced to 57.51%. This inhibitory effect is due to the scavenging effect of HCO_3^- on ·OH. Moreover, the masking product is a carbonate radical (Equation (20) [27,58]), which is a weak oxidant compared with ·OH. Meanwhile, the presence of HCO_3^- would increase the solution's pH [57], which is harmful to the activation of PAA by Fe^{2+}.
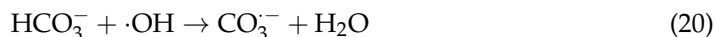
$$HCO_3^- + \cdot OH \rightarrow CO_3^{\cdot -} + H_2O \tag{20}$$

Figure 6c shows that the MB elimination in the $EC/Fe^{2+}/PAA$ was restrained through the existence of SO_4^{2-}. When the SO_4^{2-} concentration was augmented from 1 to 20 mmol L^{-1}, the MB removal ratio dropped from 98.97% to 80.79%. SO_4^{2-} would react with ·OH in the acidic environment following the production of $SO_4^{\cdot -}$ (Equation (21)) [59,60]. $SO_4^{\cdot -}$ is also a strongly oxidizing radical, so MB removal could only be restrained to a certain extent.

$$\cdot OH + SO_4^{2-} \rightarrow SO_4^{\cdot -} + OH^- \tag{21}$$
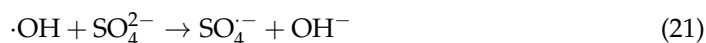
Figure 6d reveals the effect of the addition of HA on the MB removal. As expected, the MB removal efficiency was obviously reduced with the increase in HA amount. The HA could rapidly react with ·OH and R-C·, with rate constants of 2.5×10^4 L mg^{-1} s^{-1} and 5.76×10^4 L mg^{-1} s^{-1}, respectively [36], which would consume reactive species in the

$EC/Fe^{2+}/PAA$. Moreover, the presence of HA would impede the Fe^{2+} catalytic activity by the complexation of HA and Fe^{2+} [45,61], thus affecting the PAA activation for removing the MB.

3.6. Electrical Energy Analysis

Table 1 illustrates the electrical energy consumption of the EC, EC/PAA, and $EC/Fe^{2+}/$ PAA processes for removing MB, and the calculated EE/O values for the three systems were 5.601, 3.345, and 0.851 kWh/m^3, respectively. The EE/O of $EC/Fe^{2+}/PAA$ was approximately 6.58 and 3.93 times lower than those of EC and EC/PAA, respectively, which embodied an obvious decline for the power consumption, while the PAA and Fe^{2+} corresponded with the EC process. It can be deduced that the synergistic effect could not only promote the dye removal, but also markedly improve the energy efficiency.

Table 1. Electrical energy consumption for different systems.

System	E (V)	I (A)	t (min)	V (L)	Log (C_0/C)	EE/O (kWh/m^3)
EC	7.4	0.06	60	0.1	4.585	5.601
EC/PAA	6.1	0.06	60	0.1	1.094	3.345
$EC/Fe^{2+}/PAA$	6.5	0.06	60	0.1	0.739	0.851

3.7. Proposed Mechanism

Based on the aforesaid outcomes and discussion, the proposed mechanism of PAA activation for the degradation of MB using electrochemical synergy with Fe^{2+} is summarized in Figure 7. Firstly, the PAA could be activated by electron transfer on the cathode of the EC system, generating $\cdot OH$, $CH_3CO_2\cdot$, and $CH_3CO_3\cdot$. Moreover, the $\cdot OH$ generated from hydrolysis on the anode could also promote PAA activation. Secondly, the Fe^{2+} could activate PAA to produce $\cdot OH$, $CH_3CO_2\cdot$, and $CH_3CO_3\cdot$. Meanwhile, the Fe^{3+} could be persistently transformed into Fe^{2+} through the cathode reaction to encourage the circulation of Fe^{3+}/Fe^{2+}, which was conducive to the continuous activation of PAA. In addition, the cathode could donate electrons to stimulate O_2 molecules to produce $O_2^{\cdot-}$, and then generate $^1O_2$. On the other hand, the MB could lose electrons and be degraded through the anode oxidation reaction. Finally, under these radical and non-radical pathways, the dye was eliminated in the $EC/Fe^{2+}/PAA$ synergistic system.
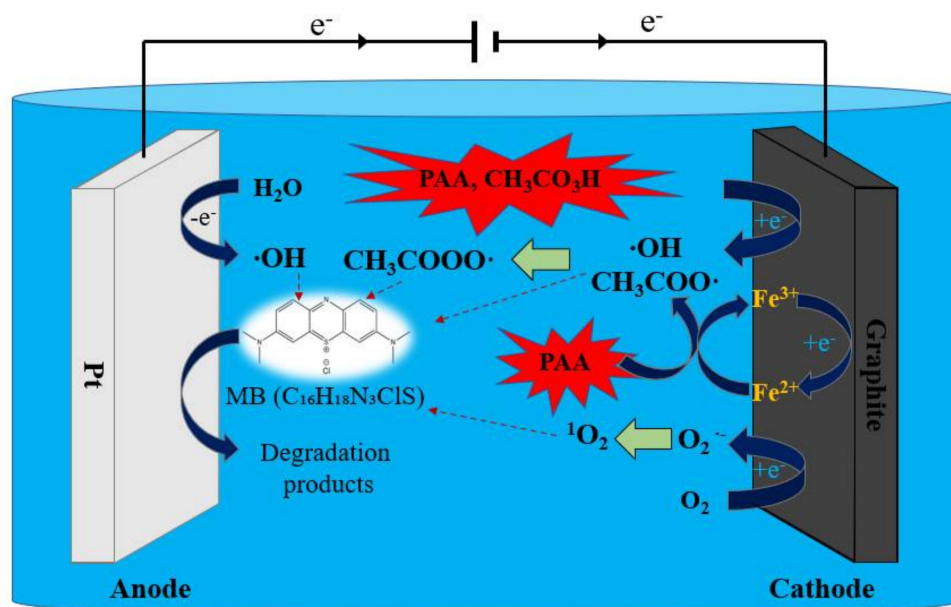
Figure 7. Possible mechanism for $EC/Fe^{2+}/PAA$ system.

4. Conclusions

A remarkable cooperative effect was generated in the electron-Fenton process for PAA activation. The effects of the operational parameters on the MB removal were optimized, and the MB decolorization efficiency reached 98.97% after 30 min under 5.4 mmol L^{-1} PAA, 30 μmol L^{-1} Fe^{2+}, 15 mA cm^{-2} current intensity, and pH 2.9. The scavenging tests proved that $\cdot OH$, $CH_3CO_2\cdot$, $CH_3CO_3\cdot$, and $^1O_2$ were the main reactive species for MB removal in the $EC/Fe^{2+}/PAA$. The PAA decomposition was greatest in the $EC/Fe^{2+}/PAA$ compared with that in the EC and EC/PAA, demonstrating the synergistic effect for PAA activation. The circulation of Fe^{3+}/Fe^{2+} can be maintained significantly with the assistance of the electric field in the $EC/Fe^{2+}/PAA$ system. The calculated EE/O results indicated that the ternary process could reduce the electrical energy consumption considerably compared to that in the EC and EC/PAA. In addition, the $EC/Fe^{2+}/PAA$ process was also used to test four other types of organic pollutants (MO, RhB, TCH, and MTZ), and they all achieved good removal effects. Therefore, the above results indicate that the $EC/Fe^{2+}/PAA$ synergistic system was a potent and dependable AOT. Furthermore, this work provides a simple and practical collaborative process for improving electrochemical oxidation technology for organic wastewater treatment.

Supplementary Materials: The following supporting information can be downloaded at: https://www.mdpi.com/article/10.3390/coatings12040466/s1, Text S1: Materials and Reagents; Text S2: Equipment and Procedure; Figure S1: UV-Vis spectrum for MB removal in $EC/Fe^{2+}/PAA$ system. Experimental conditions: $[MB]_0 = 20$ mg L^{-1}, $[Fe^{2+}]_0 = 30$ μmol L^{-1}, $[PAA]_0 = 5.4$ mmol L^{-1}, $[H_2O_2]_0 = 11.25$ mmol L^{-1}, $[NaNO_3] = 30$ mmol L^{-1}, pH = 2.9, $j = 15$ mA cm^{-2}; Figure S2: TOC removal for MB in in $EC/Fe^{2+}/PAA$ system. Experimental conditions: $[MB]_0 = 20$ mg L^{-1}, $[Fe^{2+}]_0 = 30$ μmol L^{-1}, $[PAA]_0 = 5.4$ mmol L^{-1}, $[H_2O_2]_0 = 11.25$ mmol L^{-1}, $[NaNO_3] = 30$ mmol L^{-1}, pH = 2.9, $j = 15$ mA cm^{-2}; Figure S3: HPLC-MS analysis of MB before and after reaction.

Author Contributions: Writing—original draft, K.Y.; Conceptualization, D.Y.; Writing—review and editing, D.Y., L.X., Q.H., S.T.; Investigation, E.Z., X.L., M.S.; Methodology, M.S., Q.H.; Validation, L.X.; Formal analysis, Q.H.; Project administration, S.T. All authors have read and agreed to the published version of the manuscript.

Institutional Review Board Statement: Not applicable.

Informed Consent Statement: Not applicable.

Data Availability Statement: Not applicable.

Conflicts of Interest: The authors declare no conflict of interest.

References

1. Cai, Q.Q.; Wu, M.Y.; Hu, L.M.; Lee, B.C.Y.; Ong, S.L.; Wang, P.; Hu, J.Y. Organics removal and in-situ granule activated carbon regeneration in FBR-Fenton/GAC process for reverse osmosis concentrate treatment. *Water Res.* **2020**, *183*, 116119. [CrossRef] [PubMed]
2. Zeng, S.; Smirnov, A.Y.; Borisevich, V.D.; Sulaberidze, G.A. Comparison study of schemes for separation of intermediate isotope components. *Sep. Sci. Technol.* **2020**, *55*, 2092–2098. [CrossRef]
3. Liu, J.; Huang, S.; Wang, T.; Mei, M.; Chen, S.; Li, J. Peroxydisulfate activation by digestate-derived biochar for azo dye degradation: Mechanism and performance. *Sep. Purif. Technol.* **2021**, *279*, 119687. [CrossRef]
4. Ahmad, A.; Khan, M.; Khan, S.; Luque, R.; Abualnaja, K.M.; Alduaij, O.K.; Yousef, T.A. Bio-Construction of CuO Nanoparticles Using Texas Sage Plant Extract for catalytical degradation of Methylene blue Via Photocatalysis. *J. Mol. Struct.* **2022**, *1256*, 132522. [CrossRef]
5. Duan, J.; Pang, S.; Wang, Z.; Zhou, Y.; Gao, Y.; Li, J.; Guo, Q.; Jiang, J. Hydroxylamine driven advanced oxidation processes for water treatment: A review. *Chemosphere* **2021**, *262*, 128390. [CrossRef]

6. Ahamad, T.; Naushad, M.; Alshehri, S.M. Analysis of degradation pathways and intermediates products for ciprofloxacin using a highly porous photocatalyst. *Chem. Eng. J.* **2021**, *417*, 127969. [CrossRef]

7. Stoian, M.; Maurer, T.; Lamri, S.; Fechete, I. Techniques of Preparation of Thin Films: Catalytic Combustion. *Catalysts* **2021**, *11*, 1530. [CrossRef]

8. Yuan, D.; Zhang, C.; Tang, S.; Li, X.; Tang, J.; Rao, Y.; Wang, Z.; Zhang, Q. Enhancing CaO_2 fenton-like process by Fe(II)-oxalic acid complexation for organic wastewater treatment. *Water Res.* **2019**, *163*, 114861. [CrossRef]

9. Ahamad, T.; Naushad, M.; Al-Saeedi, S.I.; Almotairi, S.; Alshehri, S.M. Fabrication of MoS_2/ZnS embedded in N/S doped carbon for the photocatalytic degradation of pesticide. *Mater. Lett.* **2020**, *263*, 127271. [CrossRef]

10. Wang, J.; Zhuan, R. Degradation of antibiotics by advanced oxidation processes: An overview. *Sci. Total Environ.* **2020**, *701*, 135023. [CrossRef]

11. Kibbee, R.; Örmeci, B. Peracetic acid (PAA) and low-pressure ultraviolet (LP-UV) inactivation of Coxsackievirus B3 (CVB3) in municipal wastewater individually and concurrently. *Water Res.* **2020**, *183*, 116048. [CrossRef]

12. Du, P.; Liu, W.; Cao, H.; Zhao, H.; Huang, C. Oxidation of amino acids by peracetic acid: Reaction kinetics, pathways and theoretical calculations. *Water Res. X* **2018**, *1*, 100002. [CrossRef]

13. Zhang, K.; Zhou, X.; Du, P.; Zhang, T.; Cai, M.; Sun, P.; Huang, C. Oxidation of β-lactam antibiotics by peracetic acid: Reaction kinetics, product and pathway evaluation. *Water Res.* **2017**, *123*, 153–161. [CrossRef]

14. Ghanbari, F.; Giannakis, S.; Lin, K.A.; Wu, J.; Madihi-Bidgoli, S. Acetaminophen degradation by a synergistic peracetic acid/UVC-LED/Fe(II) advanced oxidation process: Kinetic assessment, process feasibility and mechanistic considerations. *Chemosphere* **2021**, *263*, 128119. [CrossRef]

15. Da Silva, W.P.; Carlos, T.D.; Cavallini, G.S.; Pereira, D.H. Peracetic acid: Structural elucidation for applications in wastewater treatment. *Water Res.* **2020**, *168*, 115143. [CrossRef]

16. Ao, X.; Eloranta, J.; Huang, C.; Santoro, D.; Sun, W.; Lu, Z.; Li, C. Peracetic acid-based advanced oxidation processes for decontamination and disinfection of water: A review. *Water Res.* **2021**, *188*, 116479. [CrossRef]

17. Wang, J.; Wang, Z.; Cheng, Y.; Cao, L.; Bai, F.; Yue, S.; Xie, P.; Ma, J. Molybdenum disulfide (MoS_2): A novel activator of peracetic acid for the degradation of sulfonamide antibiotics. *Water Res.* **2021**, *201*, 117291. [CrossRef]

18. Wang, J.; Wan, Y.; Ding, J.; Wang, Z.; Ma, J.; Xie, P.; Wiesner, M.R. Thermal Activation of Peracetic Acid in Aquatic Solution: The Mechanism and Application to Degrade Sulfamethoxazole. *Environ. Sci. Technol.* **2020**, *54*, 14635–14645. [CrossRef]

19. Cai, M.; Sun, P.; Zhang, L.; Huang, C. UV/Peracetic Acid for Degradation of Pharmaceuticals and Reactive Species Evaluation. *Environ. Sci. Technol.* **2017**, *51*, 14217–14224. [CrossRef]

20. Zhang, T.; Huang, C. Modeling the Kinetics of UV/Peracetic Acid Advanced Oxidation Process. *Environ. Sci. Technol.* **2020**, *54*, 7579–7590. [CrossRef]

21. Rokhina, E.V.; Makarova, K.; Lahtinen, M.; Golovina, E.A.; Van As, H.; Virkutyte, J. Ultrasound-assisted MnO_2 catalyzed homolysis of peracetic acid for phenol degradation: The assessment of process chemistry and kinetics. *Chem. Eng. J.* **2013**, *221*, 476–486. [CrossRef]

22. Wu, W.; Tian, D.; Liu, T.; Chen, J.; Huang, T.; Zhou, X.; Zhang, Y. Degradation of organic compounds by peracetic acid activated with Co_3O_4: A novel advanced oxidation process and organic radical contribution. *Chem. Eng. J.* **2020**, *394*, 124938. [CrossRef]

23. Wang, J.; Xiong, B.; Miao, L.; Wang, S.; Xie, P.; Wang, Z.; Ma, J. Applying a novel advanced oxidation process of activated peracetic acid by $CoFe_2O_4$ to efficiently degrade sulfamethoxazole. *Appl. Catal. B-Environ.* **2021**, *280*, 119422. [CrossRef]

24. Kim, J.; Zhang, T.; Liu, W.; Du, P.; Dobson, J.T.; Huang, C. Advanced Oxidation Process with Peracetic Acid and Fe(II) for Contaminant Degradation. *Environ. Sci. Technol.* **2019**, *53*, 13312–13322. [CrossRef]

25. Kim, J.; Du, P.; Liu, W.; Luo, C.; Zhao, H.; Huang, C. Cobalt/Peracetic Acid: Advanced Oxidation of Aromatic Organic Compounds by Acetylperoxyl Radicals. *Environ. Sci. Technol.* **2020**, *54*, 5268–5278. [CrossRef]

26. Carlos, T.D.; Bezerra, L.B.; Vieira, M.M.; Sarmento, R.A.; Pereira, D.H.; Cavallini, G.S. Fenton-type process using peracetic acid: Efficiency, reaction elucidations and ecotoxicity. *J. Hazard. Mater.* **2021**, *403*, 123949. [CrossRef]

27. Chen, H.; Lin, T.; Zhang, S.; Xu, H.; Tao, H.; Chen, W. Novel FeII/EDDS/UV/PAA advanced oxidation process: Mechanisms and applications for naproxen degradation at neutral pH and low FeII dosage. *Chem. Eng. J.* **2021**, *417*, 127896. [CrossRef]

28. Xiong, L.; Ren, W.; Lin, H.; Zhang, H. Efficient removal of bisphenol A with activation of peroxydisulfate via electrochemically assisted Fe(III)-nitrilotriacetic acid system under neutral condition. *J. Hazard. Mater.* **2021**, *403*, 123874. [CrossRef]

29. Midassi, S.; Bedoui, A.; Bensalah, N. Efficient degradation of chloroquine drug by electro-Fenton oxidation: Effects of operating conditions and degradation mechanism. *Chemosphere* **2020**, *260*, 127558. [CrossRef]

30. Long, Y.; Feng, Y.; Li, X.; Suo, N.; Chen, H.; Wang, Z.; Yu, Y. Removal of diclofenac by three-dimensional electro-Fenton-persulfate (3D electro-Fenton-PS). *Chemosphere* **2019**, *219*, 1024–1031. [CrossRef]

31. Cai, J.; Zhou, M.; Du, X.; Xu, X. Enhanced mechanism of 2,4-dichlorophenoxyacetic acid degradation by electrochemical activation of persulfate on Blue-TiO_2 nanotubes anode. *Sep. Purif. Technol.* **2021**, *254*, 117560. [CrossRef]

32. Sun, Z.; Li, S.; Ding, H.; Zhu, Y.; Wang, X.; Liu, H.; Zhang, Q.; Zhao, C. Electrochemical/Fe^{3+}/peroxymonosulfate system for the degradation of Acid Orange 7 adsorbed on activated carbon fiber cathode. *Chemosphere* **2020**, *241*, 125125. [CrossRef]

33. Liu, Z.; Ren, B.; Ding, H.; He, H.; Deng, H.; Zhao, C.; Wang, P.; Dionysiou, D.D. Simultaneous regeneration of cathodic activated carbon fiber and mineralization of desorbed contaminations by electro-peroxydisulfate process: Advantages and limitations. *Water Res.* **2020**, *171*, 115456. [CrossRef]

34. Yuan, D.; Yang, K.; Pan, S.; Xiang, Y.; Tang, S.; Huang, L.; Sun, M.; Zhang, X.; Jiao, T.; Zhang, Q.; et al. Peracetic acid enhanced electrochemical advanced oxidation for organic pollutant elimination. *Sep. Purif. Technol.* **2021**, *276*, 119317. [CrossRef]

35. Yang, Z.; Yu, A.; Shan, C.; Gao, G.; Pan, B. Enhanced Fe(III)-mediated Fenton oxidation of atrazine in the presence of functionalized multi-walled carbon nanotubes. *Water Res.* **2018**, *137*, 37–46. [CrossRef]

36. Chen, S.; Cai, M.; Liu, Y.; Zhang, L.; Feng, L. Effects of water matrices on the degradation of naproxen by reactive radicals in the UV/peracetic acid process. *Water Res.* **2019**, *150*, 153–161. [CrossRef]

37. Ahmad, A.; Davarpanah, A.; Thangavelu, L.; Bokov, D.O.; Alshgari, R.A.; Karami, A.M. Self-assembled pine-like CuCo/CP configuration as efficient electrocatalysts toward electrochemical water splitting. *J. Mol. Liq.* **2022**, *351*, 118635. [CrossRef]

38. Rokhina, E.V.; Makarova, K.; Golovina, E.A.; Van As, H.; Virkutyte, J. Free Radical Reaction Pathway, Thermochemistry of Peracetic Acid Homolysis, and Its Application for Phenol Degradation: Spectroscopic Study and Quantum Chemistry Calculations. *Environ. Sci. Technol.* **2010**, *44*, 6815–6821. [CrossRef]

39. Han, S.; Hassan, S.U.; Zhu, Y.; Zhang, S.; Liu, H.; Zhang, S.; Li, J.; Wang, Z.; Zhao, C. Significance of Activated Carbon Fiber as Cathode in Electro/Fe^{3+}/Peroxydisulfate Oxidation Process for Removing Carbamazepine in Aqueous Environment. *Ind. Eng. Chem. Res.* **2019**, *58*, 19709–19718. [CrossRef]

40. Pan, S.; Zhai, Z.; Yang, K.; Xiang, Y.; Tang, S.; Zhang, Y.; Jiao, T.; Zhang, Q.; Yuan, D. β-Lactoglobulin amyloid fibrils supported Fe(III) to activate peroxydisulfate for organic pollutants elimination. *Sep. Purif. Technol.* **2022**, *289*, 120806. [CrossRef]

41. Wang, Z.; Wang, J.; Xiong, B.; Bai, F.; Wang, S.; Wan, Y.; Zhang, L.; Xie, P.; Wiesner, M.R. Application of Cobalt/Peracetic Acid to Degrade Sulfamethoxazole at Neutral Condition: Efficiency and Mechanisms. *Environ. Sci. Technol.* **2020**, *54*, 464–475. [CrossRef]

42. Pueyo, N.; Ormad, M.P.; Miguel, N.; Kokkinos, P.; Ioannidi, A.; Mantzavinos, D.; Frontistis, Z. Electrochemical oxidation of butyl paraben on boron doped diamond in environmental matrices and comparison with sulfate radical-AOP. *J. Environ. Manag.* **2020**, *269*, 110783. [CrossRef]

43. Song, H.; Yan, L.; Wang, Y.; Jiang, J.; Ma, J.; Li, C.; Wang, G.; Gu, J.; Liu, P. Electrochemically activated PMS and PDS: Radical oxidation versus nonradical oxidation. *Chem. Eng. J.* **2020**, *391*, 123560. [CrossRef]

44. Liu, J.; Zhong, S.; Song, Y.; Wang, B.; Zhang, F. Degradation of tetracycline hydrochloride by electro-activated persulfate oxidation. *J. Electroanal. Chem.* **2018**, *809*, 74–79. [CrossRef]

45. Lin, J.; Hu, Y.; Xiao, J.; Huang, Y.; Wang, M.; Yang, H.; Zou, J.; Yuan, B.; Ma, J. Enhanced diclofenac elimination in Fe(II)/peracetic acid process by promoting Fe(III)/Fe(II) cycle with ABTS as electron shuttle. *Chem. Eng. J.* **2021**, *420*, 129692. [CrossRef]

46. Wang, S.; Wang, H.; Liu, Y.; Fu, Y. Effective degradation of sulfamethoxazole with Fe^{2+}-zeolite/peracetic acid. *Sep. Purif. Technol.* **2020**, *233*, 115973. [CrossRef]

47. Cheng, X.; Guo, H.; Zhang, Y.; Wu, X.; Liu, Y. Non-photochemical production of singlet oxygen via activation of persulfate by carbon nanotubes. *Water Res.* **2017**, *113*, 80–88. [CrossRef]

48. Hama Aziz, K.H.; Mahyar, A.; Miessner, H.; Mueller, S.; Kalass, D.; Moeller, D.; Khorshid, I.; Rashid, M.A.M. Application of a planar falling film reactor for decomposition and mineralization of methylene blue in the aqueous media via ozonation, Fenton, photocatalysis and non-thermal plasma: A comparative study. *Process Saf. Environ.* **2018**, *113*, 319–329. [CrossRef]

49. Wolski, L.; Ziolek, M. Insight into pathways of methylene blue degradation with H_2O_2 over mono and bimetallic Nb, Zn oxides. *Appl. Catal. B-Environ.* **2018**, *224*, 634–647. [CrossRef]

50. Wolski, L.; Sobańska, K.; Walkowiak, A.; Akhmetova, K.; Gryboś, J.; Frankowski, M.; Ziolek, M.; Pietrzyk, P. Enhanced adsorption and degradation of methylene blue over mixed niobium-cerium oxide—Unraveling the synergy between Nb and Ce in advanced oxidation processes. *J. Hazard. Mater.* **2021**, *415*, 125665. [CrossRef]

51. Yuan, D.; Sun, M.; Tang, S.; Zhang, Y.; Wang, Z.; Qi, J.; Rao, Y.; Zhang, Q. All-solid-state $BiVO_4$/$ZnIn_2S_4$ Z-scheme composite with efficient charge separations for improved visible light photocatalytic organics degradation. *Chin. Chem. Lett.* **2020**, *31*, 547–550. [CrossRef]

52. Yuan, D.; Tang, J.; Nie, Z.; Tang, S. Study on humic acid removal in water by ultraviolet activated sodium percarbonate. *J. Yanshan Univ.* **2021**, *45*, 220–226. [CrossRef]

53. Xiang, Y.; Yang, K.; Zhai, Z.; Zhao, T.; Yuan, D.; Jiao, T.; Zhang, Q.; Tang, S. Molybdenum co-catalytic promotion for Fe^{3+}/peroxydisulfate process: Performance, mechanism, and immobilization. *Chem. Eng. J.* **2022**, *438*, 135656. [CrossRef]

54. Yin, K.; Wu, J.; Deng, Q.; Wu, Z.; Wu, T.; Luo, Z.; Jiang, J.; Duan, J. Tailoring micro/nanostructured porous polytetrafluoroethylene surfaces for dual-reversible transition of wettability and transmittance. *Chem. Eng. J.* **2022**, *434*, 134756. [CrossRef]

55. Yang, B.; Zhou, P.; Cheng, X.; Li, H.; Huo, X.; Zhang, Y. Simultaneous removal of methylene blue and total dissolved copper in zero-valent iron/H_2O_2 Fenton system: Kinetics, mechanism and degradation pathway. *J. Colloid Interface Sci.* **2019**, *555*, 383–393. [CrossRef]

56. Yuan, D.; Zhang, C.; Tang, S.; Wang, Z.; Sun, Q.; Zhang, X.; Jiao, T.; Zhang, Q. Ferric ion-ascorbic acid complex catalyzed calcium peroxide for organic wastewater treatment: Optimized by response surface method. *Chin. Chem. Lett.* **2021**, *32*, 3387–3392. [CrossRef]

57. Li, D.; Li, S.; Zhang, S.; Sun, J.; Wang, L.; Wang, K. Aging state prediction for supercapacitors based on heuristic kalman filter optimization extreme learning machine. *Energy* **2022**, *250*, 123773. [CrossRef]

58. Wang, W.; Pang, J.; Su, J.; Li, F.; Li, Q.; Wang, X.; Wang, J.; Ibarlucea, B.; Liu, X.; Li, Y.; et al. Applications of nanogenerators for biomedical engineering and healthcare systems. *InfoMat* **2022**, *4*, e12262. [CrossRef]

59. Kim, J.; Huang, C. Reactivity of Peracetic Acid with Organic Compounds: A Critical Review. *ACS EST Water* **2021**, *1*, 15–33. [CrossRef]

60. Lee, Y.; Lee, G.; Zoh, K. Benzophenone-3 degradation via UV/H$_2$O$_2$ and UV/persulfate reactions. *J. Hazard. Mater.* **2021**, *403*, 123591. [CrossRef]

61. Liu, C.; Li, Q.; Wang, K. State-of-charge estimation and remaining useful life prediction of supercapacitors. *Renew. Sustain. Energy Rev.* **2021**, *150*, 111408. [CrossRef]